# Seeing Is Believing: Hot Electron Based Gold Nanoplasmonic Optical Hydrogen Sensor

Devika Sil,[†] Kyle D. Gilroy,[‡] Aurelia Niaux,[†] Abdelaziz Boulesbaa,[†] Svetlana Neretina,[‡] and Eric Borguet[†,*]

[†]Department of Chemistry, Temple University, Philadelphia, Pennsylvania 19122, United States and [‡]College of Engineering, Temple University, Philadelphia, Pennsylvania 19122, United States

ABSTRACT We report on the rapid optical detection of gaseous hydrogen using hot electrons generated from resonantly excited substrate-based gold nanohemispheres (Au NHs). We consider hot electron induced H_2 dissociation and the subsequent formation of a metastable gold hydride (AuH_x) to account for changes in optical transmission. The excitation wavelength was varied to demonstrate a maximum response at the localized surface plasmon resonance (LSPR) wavelength of the AuNHs. Numerical simulations, using the discrete dipole approximation, were employed to corroborate the optical changes associated with the formation of metastable AuH_x. Finite time difference domain (FDTD) calculations were also performed to account for the enhanced photocatalytic activity arising due to the confinement of electric fields by the Au NHs. FDTD simulations show that the excitation of the Au NHs plasmon modes generates stronger electric fields at the interface in comparison to a spherical geometry of similar dimensions.
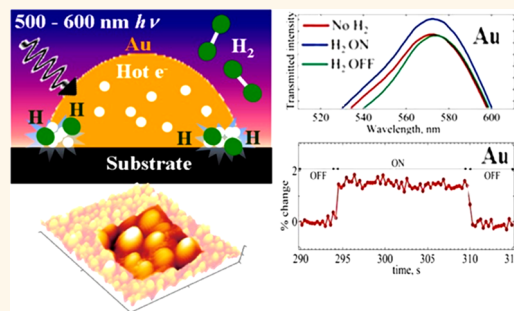
KEYWORDS: hydrogen · optical · detection · surface plasmons · hot electrons · gold

The interaction of metal nanoparticles (NPs) with photons whose energy is resonant with the surface plasmon leads to the generation of plasma oscillations which can decay into hot electrons.[1−3] This strong interaction offers the opportunity to couple light to drive chemical reactions and provides a means to generate valuable product with relatively low energy input.[2] The probability of generating thermalized, or "hot", electrons is increased when the metal nanoparticles are much smaller than the wavelength of the incident radiation.[2]

Recent studies have focused on the transfer of hot electrons from excited metal surfaces to nearby molecular orbitals.[2,3] Mukherjee et al. provided the first experimental evidence for the room-temperature photocatalytic dissociation of H_2 on 5−30 nm gold nanoparticles using visible light.[2,3] Their results demonstrated that a fraction of the hot electrons generated by the resonantly excited gold nanoparticles allowed for electron transfer into the $1\sigma_u$* antibonding orbital of a physisorbed H_2 molecule, leading to

dissociation.[2,3] The requirements for this process are that (i) the Au NPs are excited resonantly, (ii) the Feshbach energy overlaps the hot electron distribution,[4] (iii) the hot electrons have energy greater than 1.8 eV, (iv) the weight fraction of Au in TiO_2, or SiO_2, is between 0.5% and 3%,[2,3] and (v) the nanoparticles are sufficiently small (<10 nm)[2] in order to maximize the surface to volume ratio and increase the fraction of lower coordination, highly reactive surface atoms.[5] Thus, the presence of these thermalized carriers makes the otherwise inert surface of Au reactive. Hot electrons have been used in a variety of other applications, e.g., oxidation of ethylene on Ag nanocubes,[6] water splitting,[7,8] solar energy harvesting,[9] sensing,[10,11] catalysis,[2,12] generation of H_2 from alcohol,[4] hydrocarbon conversion,[13] the fabrication of novel molecular electronic devices,[14] plasmonic switches,[15] and nanoscale electronics.[16]

Before the hot electron induced dissociative capabilities of Au nanoparticles were realized and used for sensing by Mukherjee et al.,[2] an indirect nanoplasmonic sensing

scheme using the localized surface plasmon resonance (LSPR) was reported.[17−23] The LSPR is a sensitive probe of changes in the local environment, such as perturbations in the dielectric properties of the medium. The collective oscillations of free electrons are driven by the interaction of plasmonic metallic nanoparticles (typically Au, Ag, or Cu) with visible light.[24] Indirect nanoplasmonic sensing schemes employ an enhanced electric field to sense changes in the dielectric environment triggered by a secondary active material, such as Pd. When placed in the near-field of resonantly excited Au nanoparticles, an external analyte molecule (e.g., H_2) changes the dielectric properties of Pd, which in turn shifts the LSPR of the Au nanoparticles.[17−23] Pd was chosen due to its well-established ability to dissociate and absorb hydrogen and undergo a reversible lattice expansion.[25,26] As shown by Liu et al., as the Pd NP approaches the near-field of a resonantly excited Au nanotriangle, the spectral position and scattering intensity of the Au system shift upon hydrogen exposure due to the formation of Pd hydride, which has different dielectric properties compared to Pd.[22] Langhammer et al. used substrate-based Au nanodisks separated from Pd nanoparticles by a thin dielectric spacer layer to study hydriding and dehydriding kinetics of 1.8−5.4 nm Pd nanoparticles.[23] However, Liu et al. and Langhammer et al. did not report any hydrogen sensing with the Au nanostructures alone.[22,23] The discovery of the hot electron induced photocatalytic activity of Au nanoparticles by Mukherjee et al.[2,3] shows that the Au LSPR could drive the dissociation of H_2 without the need for an adjacent active material such as Pd. However, any change in the optical response of the Au nanoparticles due to hot electron induced dissociation of hydrogen has yet to be reported.

The interaction of Au with hydrogen, especially the formation of Au−H bonds, is far from being understood due to the inert nature of bulk Au. However, there are studies, both theoretical and experimental, that discuss the adsorption of hydrogen onto Au[27−30] and the formation of AuH_x.[30−37] Bus et al. reported that small gold nanoparticles (∼1.4 nm) supported on alumina dissociatively adsorb hydrogen.[30] This is accompanied by a change in electronic properties, as it was shown by X-ray absorption near-edge spectroscopy that the $L_{3,2}$ edges of Au/Al_2O_3 recorded in hydrogen undergo a shift of several electronvolts.[30] Previous reports also mentioned that the formation of surface-based $AuH_2^−$ and $AuH_4^−$ is stabilized by relativistic effects[38] and is likely to occur in electron-rich systems such as provided by laser ablation and plasmas.[34] The catalytic activity was associated with atomic sites of lower coordination (i.e., at the edges and corners).

In this work, we optically detect the dissociation of H_2 on Au nanoparticles. The novelty stems from the room-temperature optical detection of hydrogen using (i) thermally self-assembled substrate-based gold nanohemispheres (Au NHs) and (ii) surfactant-free structures (allowing for close contact between the nanostructures and the analyte). It is important to note that the observation of hot electron generation for spherical, larger nanostructures (>20 nm) was previously reported to be negligible[2,4,39] and that the dissociation of H_2 was negligible.[2,4,40,41] On the contrary, in the present study, a ∼1−2% change in optical transmission was achieved at room temperature using Au NHs between 10 and 50 nm in diameter upon incoherent excitation. To substantiate the claim of AuH_x formation, discrete dipole approximation (DDA) simulations were carried out using dielectric constants of Au hydride previously measured by Giangregorio et al.[34]

RESULTS

Characterization of Films. Tapping mode atomic force microscope (AFM) images of the Au NHs film (Figure 1a) showed a broad distribution of closely spaced hemispherical particles between 10 and 50 nm. A histogram is shown in Figure 1b, where the average size was measured to be ∼28 ± 8 nm. The UV/vis extinction spectrum (Figure 1c) showed the plasmon band of Au NHs as a wide inhomogeneously broadened feature at ∼570 nm. The peak position appeared to be red-shifted by about 50 nm from the previously reported position of plasmon band for spherical Au NPs.[42] This shift in spectral position of the plasmon band could be attributed to two effects: (a) nanoparticle shape induced effects and (b) nanoparticle size related changes in surface plasmon resonance. The geometry-induced shift was observed previously for other metals[43] and was attributed to the effective dipole being closer to the substrate. It was found that hemispheres have a stronger interaction with the substrate as compared to spheres.[43,44] Nanoparticle dimension induced changes in the surface plasmon resonance arise due to increased electromagnetic retardation in larger nanoparticles.[45,46] In the present case, the red shift could be a cumulative result of the two aforementioned phenomena.

Plasmonic Sensing Results. The broadband incoherent excitation was selected to cover wavelengths between 500−600 nm and the real time response of the Au film (Figure 2a−c) in H_2 was monitored. An average increase of ∼1.8% in the transmitted intensity through an Au NH film, supported on a glass slide, was observed within 0.3−1 s of turning on H_2. The Au NH film was exposed to 10% H_2 in N_2 for 10−20 s, during which time the transmitted intensity stayed constant. Upon turning off the H_2 flow, the transmitted intensity recovered to the initial value. Thus, from the real-time monitoring of the response of Au NHs to H_2 (Figure 2), it became evident that these nanostructures act as rapid and reusable optical H_2 sensors upon resonant excitation at the SPR. Details regarding the experimental setup are provided in the Supporting Information (SI, Figure S1).
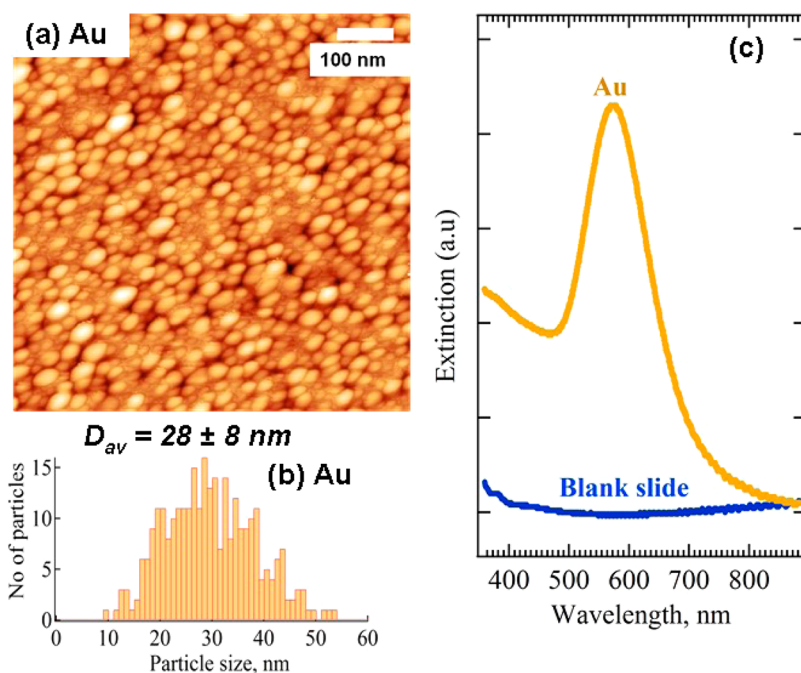
Figure 1. Morphological and optical characterization of a thermally assembled Au film. Morphological characterization using tapping mode AFM on (a) dewetted Au NHs and (b) histogram showing particle size distribution of Au NHs, with an average size of 28 ± 8 nm. (c) UV/vis extinction spectra of the Au NH film and of a blank slide.
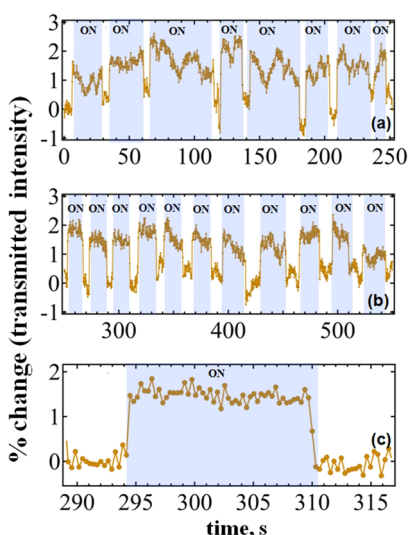

Figure 2. Real-time monitoring of changes in transmitted intensity for multiple cycles of H_2. Each point plotted is the percentage change in transmitted intensity between 500 and 600 nm as a function of time. Each time increment was 0.3 s apart. Rapid response after (a) seven cycles of hydrogen, (b) 11 cycles of hydrogen, and (c) one cycle of hydrogen close up to show both the ON and OFF response.

Hydriding and Dehydriding of Au NHs with UV/Vis Spectroscopy. The surface plasmon resonance of Au NHs films was tracked with and without hydrogen exposure by recording transmission spectra with a UV/vis spectrometer. In the absence of hydrogen the signal stayed stable at a transmittance of ∼46%. Upon introducing hydrogen, a ∼1% increase in transmittance was
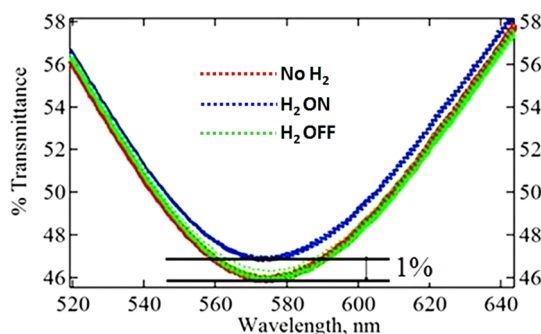

Figure 3. Tracking the surface plasmon resonance of Au NHs in H_2 with a UV/vis spectrometer. Red spectrum is without any H_2; blue spectrum displays the optical response during hydrogen; and green is after the hydrogen is stopped. The presence of hydrogen causes a reversible 1% change in transmittance.

observed (Figure 3). After stopping H_2 and waiting, the transmittance signal recovered to the initial value. The presence of hydrogen induced a blue shift of ∼3 nm.

Wavelength Dependence. Combinations of filters were placed in the beam path to vary the incident excitation wavelength range (See Figure S4 in SI for details) in order to study how it affected the magnitude of the optical response of the Au NH films to hydrogen. The experiments were carried out at 293 K and under similar illumination intensities covering photon wavelengths from 400−800 nm. The change in transmission was greatest for wavelengths within 30 nm of the LSPR (λ_{ex} = 550 and 580 nm) (Figure 4).
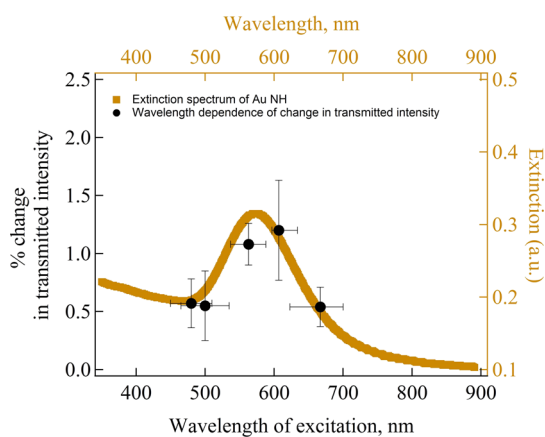
Figure 4. Effect of excitation wavelength on the magnitude of change in the transmission of Au films in hydrogen. Excitations within 50 nm of the LSPR of Au NHs (570 nm) demonstrate larger changes in transmittance. The LSPR of the Au NH film is indicated by the yellow dotted line.

DISCUSSION

The question as to why Au nanoparticle surfaces are reactive to hydrogen when their LSPR is excited was recently answered by Mukherjee et al.[2] They provided a mechanism of hot electron induced dissociation of hydrogen on Au nanoparticles and showed the formation of HD from a constant flow of H_2 and D_2 on supported Au catalysts. On the basis of the mechanism put forward by Mukherjee et al.[2] and the agreement of experimental observations with theoretical calculations, we believe the optical change could be happening through the following steps:

(a) Optical excitation is resonant with the LSPR of Au nanoparticles

(b) Coherent plasmons decay into hot electrons

(c) A fraction of the hot electrons undergo electron transfer into the H_2 $1\sigma_u^*$ antibonding orbital, which leads to H_2 dissociation

(d) Dissociated hydrogen atoms adsorb and diffuse into Au NHs to form a metastable Au hydride

$$Au + H_2 \rightarrow Au - H \quad (1)$$

$$Au - H + H \rightarrow Au + H_2\uparrow \quad (2)$$
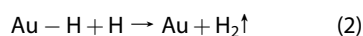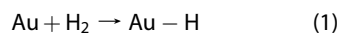
(e) Metastable Au hydride has a different dielectric constant than Au. The change in dielectric constants modifies the LSPR position of the particles and the optical transmission of the thin film.

(f) In the absence of a steady flux of H_2, there is a net diffusion of H atoms out from nanoparticle thin film leading to recovery of the initial optical properties.

The formation of the metastable Au hydride induces a spectral shift and change in transmitted intensity, which are explained as follows:

Spectral Shift in Au LSPR in the Presence of Hydrogen Due to Electron Transfer. The surface plasmon resonance

condition is approximately fulfilled when

$$\varepsilon_1 = -2\varepsilon_m \quad (3)$$

where ε_1 is the real part of the dielectric constant of the metal and ε_m is the dielectric constant of the embedding medium of the nanoparticles.[34] The Drude model predicts that the dielectric constants of metals depend on the plasmon frequency as follows:

$$\varepsilon_D(\omega) = 1 - \frac{\omega_p^2}{\omega^2 + i\gamma\omega} \quad (4)$$

where

$$\omega_p^2 = \frac{ne^2}{\varepsilon_0 m_{eff}} \quad (5)$$

ω_p is the plasmon frequency, γ is the damping constant, n is the electron density, e is the electron charge, ε_o is the permittivity in a vacuum, and m_{eff} is the effective mass of the electron. Since the plasmon frequency varies as the square root of electron density, any change in the number of electrons (*i.e.*, addition or removal of electrons from the metallic core) will shift the position of the surface plasmon resonance. Therefore, a blue shift in the position of the surface plasmon upon hydrogenation implies an increase in electron density, hence a more negative dielectric constant, which is consistent with the slight spectral shift of 3 nm observed in Au LSPR in H_2 (Figure 3). Our optical simulations also show that, in order to observe a 1% increase in transmission and a 3 nm blue shift in Au NH LSPR due to hydrogenation, the real and imaginary parts of the dielectric constant of Au need to change by roughly 2% (SI, Figure S3). Therefore, the probability of the presence of a metastable Au hydride with dielectric constants different than pure Au due to adsorption of hydrogen cannot be ruled out.

Au hydride was observed by Strobiriski et al. and Bus et al.[36,47] Thus, based on the change in transmission and the blue shift of Au (Figures 2, 3) in hydrogen and agreement with optical calculations (SI, Figure S3), we speculate that the change in optical transmission results from the formation of a metastable gold hydride due to the adsorption of hydrogen atoms.

Wavelength Dependence of Magnitude of Change in Optical Transmission. The dependence of the magnitude of the optical change on the wavelength of excitation is also a major indicator of a plasmon-driven chemical process.[2,3,6] Therefore, the excitation wavelengths were tuned in order to excite at various photon energies (Figure 4) close (within 30 nm) and far (70−100 nm) from the LSPR peak of Au NH. Our results show that when the central wavelength of excitation was within 30 nm of the LSPR, the optical transmission increased by ∼1−2%. Upon excitation with wavelengths further away (70−100 nm) from the peak of the LSPR, the magnitude of the optical change in transmission is less, typically a factor of 4 lower. Outside this window of
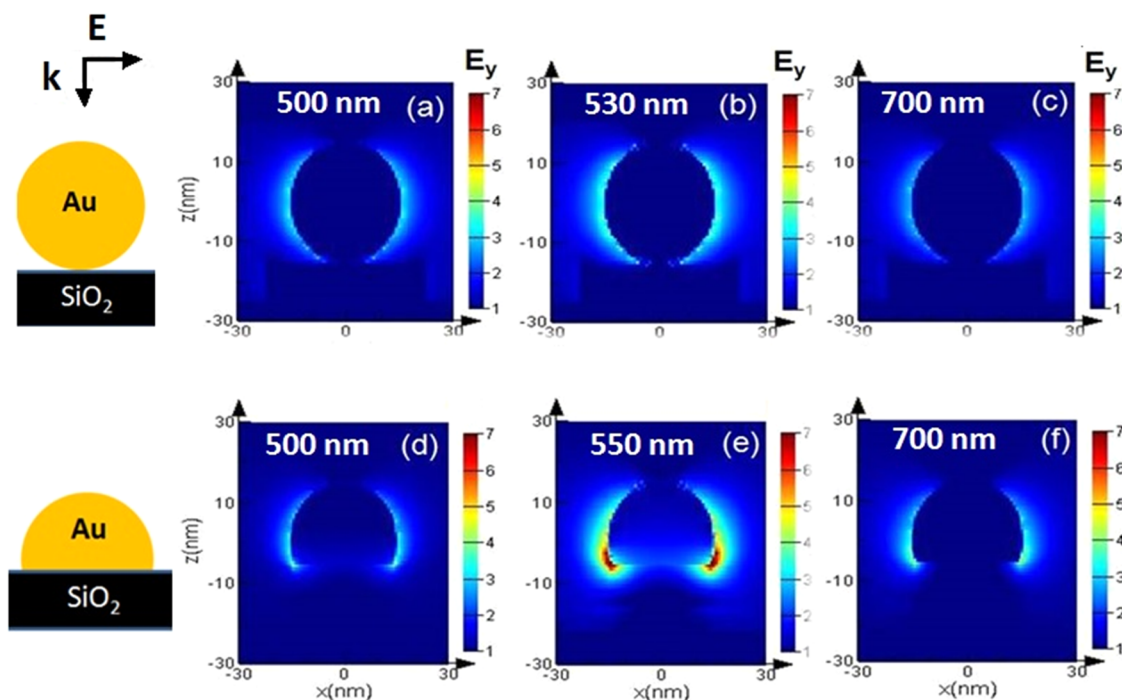
Figure 5. FDTD-simulated electric fields at different wavelengths for an SiO$_2$ substrate with a single Au sphere on (a,b,c) or a single Au hemisphere (d,e,f). The near field enhancements for the Au sphere on the SiO$_2$ substrate were computed at (a) 500 nm (b) 530 nm-LSPR (c) 700 nm. The near field enhancements for the Au hemisphere on SiO$_2$ were calculated at (d) 500 nm (e) 550 nm-LSPR (f) 700 nm. Schematics on the left show the geometry used for the simulation as well as the orientation of the incident k-vector (normal to the surface) and the E-field (y component). At 530 nm, a 1.3× enhancement was observed for the 30 nm Au sphere. At 550 nm, a 2.3× enhancement was observed at the edge of the hemisphere. Au NHs showed about 1.75× more resonant E-field enhancement in comparison to the sphere at the LSPR.

near-resonant photon energies, smaller changes are observed due to a variety of reasons including (i) fewer hot electrons are generated and (ii) the $(e^- - H_2)$ interaction probability is low. Mukherjee et al. observed similar results for plasmonic HD generation and mentioned that "since the absorption cross section corresponds directly to the hot electron production rate, this provides direct evidence for plasmon-induced hot-electron-driven H$_2$ photodissociation".[2] Christopher et al. also reported similarity in the wavelength dependence of ethylene epoxidation rates due to dissociation of oxygen on Ag nanocubes and the LSPR spectrum of the silver nanocube catalysts used.[6] This correlation between the wavelength dependence of plasmon-induced reactions and the LSPR spectrum of metallic nanocatalysts at constant illumination intensity provides evidence that the resonant LSPR excitation is responsible for the photocatalytic activity.

Confinement of the Electric Field. Finite difference time domain (FDTD) simulations were performed to identify the origin of the photocatalytic response of large (>20 nm) Au NHs. We compared the nature of the electric field enhancement of substrate-based Au spheres and Au NHs, both 30 nm in diameter, using FDTD. The simulation (Figure 5) demonstrated that, upon resonant excitation, the Au NHs generate strong fields near the surface of the substrate. The Au NHs exhibit maximum enhancement at ~550 nm

(Figure 5e), which is the calculated surface plasmon resonance of a 30 nm Au hemisphere positioned on SiO$_2$. The UV/vis spectrum of Au NHs showed a plasmon resonance at 570 nm. This red shift could be attributed to the presence of larger particles arising from the polydispersity in nanoparticle size distribution. The spherical Au nanoparticles exhibited the maximum enhancement of 1.3 times at 530 nm (Figure 5b) at the LSPR wavelength. On the other hand, the 30 nm Au NHs showed 2.3 times enhancement at its LSPR (570 nm) (Figure 5e). It was evident that off-resonance, e.g., 500 and 700 nm (Figure 5a, c, d, f), the electric field was weaker than at the LSPR for both geometries. The Au NHs exhibited approximately twice as much confinement of the electric field as the spheres of similar dimensions. The confinement in the hemisphere was localized at the interface with the substrate, which we suggest is the hot spot for the plasmon-induced reactions reported here.

Absence of Surfactants or Ligands. Another factor that possibly enhances the efficiency of the hot electron induced dissociation is the absence of any surfactants or ligands on the thermally dewetted Au NHs. The rate of hot electron cooling determines the lifetime of the energetic electrons and is known to depend on the electronic heat capacity and the magnitude of electron−phonon coupling. Aruda et al. described how the hot electron cooling process is affected by the

presence of an organic adlayer on a nanoparticle.[1,48] The electronic states of metals are known to mix with that of organic adsorbates, making the density of states of passivated metal nanoparticles considerably different from that of the bulk. Such intermixing of electronic states can significantly alter the electronic heat capacity. A summary of prior investigations on this effect can be found in Aruda *et al.*[1] The magnitude of electron−phonon coupling also varies from material to material and is also dependent on the density of electronic states of the system near the Fermi level and the distribution of vibrational modes. Therefore, any adsorption of ligands or surfactants or changes in lattice structure will influence the hot electron cooling rate.[1] Since our system is relatively simple, devoid of any protective layer, the hot electron lifetime is most likely unaffected, which in turn induces efficient hydrogen dissociation on Au. This makes the resonantly excited Au surface more responsive to hydrogen.

Probable Presence of Defects. Another factor that could contribute to the enhanced activity of Au NHs is the presence of twin boundaries or stacking faults, which are usually present in Au nanoparticles of similar dimensions.[49] The presence of such defects are known to enhance catalytic activity by lowering the dissociation barrier.[49−51] Thus, the enhanced reactivity of the Au NHs could be due to the combined effects of the geometry, the absence of surfactants, and the presence of defects.

CONCLUSION

In this work, we demonstrated that thermally assembled Au NHs provide a platform for the plasmonic detection of H_2. It was also concluded that plasmonic detection of H_2 was primarily contingent upon the resonant excitation of the localized surface plasmons. Investigations into wavelength dependence showed that resonantly excited Au NHs show the greatest increase in hydrogen-induced optical transmission, confirming the electronic origin of the response. Numerical simulations support the assertion that the formation of a metastable AuH_x can change the dielectric properties of the films enough to be detected optically. To conclude, we believe that the simplicity of this optical detection system, coupled with the ability to observe small changes occurring on subsecond time scales under equilibrium conditions, will open up other sensing possibilities.

MATERIALS AND METHODS

Preparation of Au NH Films. Substrate-based Au nanostructures were produced using thermal dewetting.[52] This process involves two steps: (i) sputter deposition (Gatan high resolution ion beam coater model 681) of a 10 nm Au thin film onto sodalime silica microscope glass slides (the resultant film is blue in color) and then (ii) heating from room temperature to 500 °C in 15 min (Lindberg Blue M tube furnace, TF55035A-1) followed by cooling back to room temperature. All samples were heated in a constant flow of ultra high purity argon at 65 sccm. The assembled Au nanostructures have a hemispherical morphology and are pink in color.[52]

Characterization. The morphology of Au NHs was assessed using AFM tapping mode images recorded using an Agilent 5500 scanning probe microscope with Si_3N_4 tips (Vista Probes) and processed using Gwyddion software.[53] The histograms were computed using ImageJ (NIH) on a minimum of 100 randomly selected nanoparticles. UV/vis spectroscopy was carried out using a JASCO V570 spectrophotometer for the characterization of optical extinction. An Evolution 201 UV/vis spectrometer was used to study spectral behavior of hydriding and dehydriding of Au nanoparticles (wavelength range 190−700 nm, bandwidth 1 nm, integration time 0.1 s, data interval 1 nm, scan speed 600 nm/min).

Simulation of Optical Properties. Simulations were done using DDSCAT 7.2.0 to explain the changes in dielectric constants of Au upon hydrogenation.[54] DDSCAT is a software package that uses numerical methods to solve for an object's optical response (*i.e.*, absorption and scattering). It uses a 3D array of polarizable points to represent the simulated continuum. The key parameters are (i) the optical properties of the material and surroundings and (ii) the object's geometry. In this case, dielectric coefficients for Au were taken from Palik.[55] The dielectric constants of AuH_x were previously measured values reported by Giangregorio *et al.*[34]

The hemispherical file was modeled using LAMMPS Molecular Dynamics Simulator[56] and was designed so that the incident photon will penetrate directly through the top of the structure, as would be done in the experiment. The E-field is oscillating parallel to the substrate, while the k-vector is perpendicular. The structure was modeled using $N > 50k$ dipoles. The effective radius of the structure is 40 nm, which is equivalent to a hemisphere with a 44.7 nm radius, yielding an LSPR centered at 561 nm.

Electromagnetic Simulation. Three-dimensional finite difference time domain methods (Lumerical FDTD Solutions) were used to calculate the near-field properties of resonantly excited Au spheres and hemispheres. Nanoparticles with 30 nm diameter were chosen to closely match experimental conditions. A mesh size of 0.8 nm was chosen for all cases. The simulated excitation source took the form of a polarized Mie source (500−700 nm) penetrating the structure with a k-vector normal to the substrate surface.

Experimental Setup. The details about the optical sensing setup can be found in the SI (Figure S1).

Conflict of Interest: The authors declare no competing financial interest.

Supporting Information Available: Figure S1 describes the experimental setup, Figure S2 shows the plots of real and imaginary parts of the refractive index of Au and AuH_x, Figure S3 is simulation of extinction spectra of Au and Au hydride, and Figure S4 shows the spectrum of the filters used for the wavelength dependence study. This material is available free of charge *via* the Internet at http://pubs.acs.org.

REFERENCES AND NOTES

1. Aruda, K. O.; Tagliazucchi, M.; Sweeney, C. M.; Hannah, D. C.; Weiss, E. A. The Role of Interfacial Charge Transfer-Type Interactions in the Decay of Plasmon Excitations in Metal Nanoparticles. *Phys. Chem. Chem. Phys.* **2013**, *15*, 7441–7449.

2. Mukherjee, S.; Libisch, F.; Large, N.; Neumann, O.; Brown, L. V.; Cheng, J.; Lassiter, J. B.; Carter, E. A.; Nordlander, P.; Halas, N. J. Hot Electrons Do the Impossible: Plasmon-Induced Dissociation of H_2 on Au. *Nano Lett.* **2012**, *13*, 240–247.

3. Mukherjee, S.; Zhou, L.; Goodman, A. M.; Large, N.; Ayala-Orozco, C.; Zhang, Y.; Nordlander, P.; Halas, N. J. Hot-Electron-Induced Dissociation of H_2 on Gold Nanoparticles Supported on SiO_2. *J. Am. Chem. Soc.* **2014**, *136*, 64–67.

4. Murdoch, M.; Waterhouse, G. I. N.; Nadeem, M. A.; Metson, J. B.; Keane, M. A.; Howe, R. F.; Llorca, J.; Idriss, H. The Effect of Gold Loading and Particle Size on Photocatalytic Hydrogen Production from Ethanol over Au/TiO_2 Nanoparticles. *Nat. Chem.* **2011**, *3*, 489–492.

5. Bastus, N. G.; Casals, E.; Ojea, I.; Varon, M.; Puntes, V. The Delivery of Nanoparticles. In *The Reactivity of Colloidal Inorganic Nanoparticles*; Hashim, D. A. A., Ed.; InTech, 2012; pp 377−401.

6. Christopher, P.; Xin, H.; Linic, S. Visible-Light-Enhanced Catalytic Oxidation Reactions on Plasmonic Silver Nanostructures. *Nat. Chem.* **2011**, *3*, 467–472.

7. Mubeen, S.; Lee, J.; Singh, N.; Krämer, S.; Stucky, G. D.; Moskovits, M. An Autonomous Photosynthetic Device in Which All Charge Carriers Derive from Surface Plasmons. *Nat. Nanotechnol.* **2013**, *8*, 247–251.

8. Thomann, I.; Pinaud, B. A.; Chen, Z.; Clemens, B. M.; Jaramillo, T. F.; Brongersma, M. L. Plasmon Enhanced Solar-to-Fuel Energy Conversion. *Nano Lett.* **2011**, *11*, 3440–3446.

9. Schwede, J. W.; Bargatin, I.; Riley, D. C.; Hardin, B. E.; Rosenthal, S. J.; Sun, Y.; Schmitt, F.; Pianetta, P.; Howe, R. T.; Shen, Z.-X. Photon-Enhanced Thermionic Emission for Solar Concentrator Systems. *Nat. Mater.* **2010**, *9*, 762–767.

10. Renzas, J. R.; Somorjai, G. A. Rh Thin-Film Nanocatalysts as Chemical Sensors−the Hot Electron Effect. *J. Phys. Chem. C* **2010**, *114*, 17660–17664.

11. Joy, N. A.; Janiszewski, B. K.; Novak, S.; Johnson, T. W.; Oh, S.-H.; Raghunathan, A.; Hartley, J. G.; Carpenter, M. A. Thermal Stability of Gold Nanorods for High-Temperature Plasmonic Sensing. *J. Phys.Chem. C* **2013**, *117*, 11718–11724.

12. Maillard, M.; Huang, P.; Brus, L. Silver Nanodisk Growth by Surface Plasmon Enhanced Photoreduction of Adsorbed $[Ag^+]$. *Nano Lett.* **2003**, *3*, 1611–1615.

13. Hou, W.; Hung, W. H.; Pavaskar, P.; Goeppert, A.; Aykol, M.; Cronin, S. B. Photocatalytic Conversion of Co_2 to Hydrocarbon Fuels *via*Plasmon-Enhanced Absorption and Metallic Interband Transitions. *ACS Catal.* **2011**, *1*, 929–936.

14. Conklin, D.; Nanayakkara, S.; Park, T.-H.; Lagadec, M. F.; Stecher, J. T.; Chen, X.; Therien, M. J.; Bonnell, D. A. Exploiting Plasmon-Induced Hot Electrons in Molecular Electronic Devices. *ACS Nano* **2013**, *7*, 4479–4486.

15. Wu, F.; Tian, L.; Kanjolia, R.; Singamaneni, S.; Banerjee, P. Plasmonic Metal-to-Semiconductor Switching in Au Nanorod-ZnO Nanocomposite Films. *ACS Appl. Mater. Interfaces* **2013**, *5*, 7693–7697.

16. Li, C.; Zhang, Y.; Cole, M. T.; Shivareddy, S. G.; Barnard, J. S.; Lei, W.; Wang, B.; Pribat, D.; Amaratunga, G. A. J.; Milne, W. I. Hot Electron Field Emission *via* Individually Transistor-Ballasted Carbon Nanotube Arrays. *ACS Nano* **2012**, *6*, 3236–3242.

17. Pavan Kumar, G. V.; Raghuwanshi, M. Palladium Adjoined Gold Split-Ring Resonators: A Prospective Nanoplasmonic Hydrogen Sensor. *Opt. Commun.* **2013**, *300*, 65–68.

18. Dasgupta, A.; Kumar, G. V. Palladium Bridged Gold Nanocylinder Dimer: Plasmonic Properties and Hydrogen Sensitivity. *Appl. Opt.* **2012**, *51*, 1688–1693.

19. Tang, M. L.; Liu, N.; Dionne, J. A.; Alivisatos, A. P. Observations of Shape-Dependent Hydrogen Uptake Trajectories from Single Nanocrystals. *J. Am. Chem. Soc.* **2011**, *133*, 13220–13223.

20. Shegai, T.; Johansson, P.; Langhammer, C.; Käll, M. Directional Scattering and Hydrogen Sensing by Bimetallic Pd-Au Nanoantennas. *Nano Lett.* **2012**, *12*, 2464–2469.

21. Tittl, A.; Kremers, C.; Dorfmuller, J.; Chigrin, D. N.; Giessen, H. Spectral Shifts in Optical Nanoantenna-Enhanced Hydrogen Sensors. *Opt. Mater. Express* **2012**, *2*, 111–118.

22. Liu, N.; Tang, M. L.; Hentschel, M.; Giessen, H.; Alivisatos, A. P. Nanoantenna-Enhanced Gas Sensing in a Single Tailored Nanofocus. *Nat. Mater.* **2011**, *10*, 631–636.

23. Langhammer, C.; Zhdanov, V. P.; Zorić, I.; Kasemo, B. Size-Dependent Kinetics of Hydriding and Dehydriding of Pd Nanoparticles. *Phys. Rev. Lett.* **2010**, *104*, 135502.

24. Kelly, K. L.; Coronado, E.; Zhao, L. L.; Schatz, G. C. The Optical Properties of Metal Nanoparticles: The Influence of Size, Shape, and Dielectric Environment. *J. Phys. Chem. B* **2003**, *107*, 668–677.

25. Flanagan, T. B.; Oates, W. A. The Palladium-Hydrogen System. *Annu. Rev. Mater. Sci.* **1991**, *21*, 269–304.

26. Lewis, F. A. *The Palladium Hydrogen System*; Academic Press: London, 1967; Vol. 124.

27. Wang, Y.; Gong, X. G. First-Principles Study of Interaction of Cluster Au32 with CO, H_2, and O_2. *J. Chem. Phys.* **2006**, *125*.

28. Csonka, S.; Halbritter, A.; Mihaly, G.; Jurdik, E.; Shklyarevskii, O.; Speller, S.; Van Kempen, H. Fractional Conductance in Hydrogen-Embedded Gold Nanowires. *Phys. Rev. Lett.* **2003**, *90*, 116803.

29. Jelínek, P.; Pérez, R.; Ortega, J.; Flores, F. Hydrogen Dissociation over Au Nanowires and the Fractional Conductance Quantum. *Phys. Rev. Lett.* **2006**, *96*, 046803.

30. Bus, E.; Miller, J. T.; van Bokhoven, J. A. Hydrogen Chemisorption on Al_2O_3-Supported Gold Catalysts. *J. Phys. Chem. B* **2005**, *109*, 14581–14587.

31. Driessen, A.; Sanger, P.; Hemmes, H.; Griessen, R. Metal Hydride Formation at Pressures up to 1 Mbar. *J. Phys.: Condens. Matter* **1990**, *2*, 9797.

32. McLellan, R. Solid Solutions of Hydrogen in Gold, Silver and Copper. *J. Phys. Chem. Solids* **1973**, *34*, 1137–1141.

33. Schmidbaur, H.; Raubenheimer, H. G.; Dobrzańska, L. The Gold−Hydrogen Bond, Au−H, and the Hydrogen Bond to Gold, AuH−X. *Chem. Soc. Rev.* **2014**, *43*, 345–380.

34. Giangregorio, M. M.; Losurdo, M.; Bianco, G. V.; Operamolla, A.; Dilonardo, E.; Sacchetti, A.; Capezzuto, P.; Babudri, F.; Bruno, G. Insight into Gold Nanoparticle−Hydrogen Interaction: A Way to Tailor Nanoparticle Surface Charge and Self-Assembled Monolayer Chemisorption. *J. Phys. Chem. C* **2011**, *115*, 19520–19528.

35. Kang, G.-J.; Chen, Z.-X.; Li, Z.; He, X. A Theoretical Study of the Effects of the Charge State and Size of Gold Clusters on the Adsorption and Dissociation of H_2. *J. Chem. Phys.* **2009**, *130*, 034701.

36. Bus, E.; van Bokhoven, J. A. Hydrogen Chemisorption on Supported Platinum, Gold, and Platinum−Gold-Alloy Catalysts. *Phys. Chem. Chem. Phys.* **2007**, *9*, 2894–2902.

37. Boronat, M.; Concepción, P.; Corma, A.; González, S.; Illas, F.; Serna, P. A Molecular Mechanism for the Chemoselective Hydrogenation of Substituted Nitroaromatics with Nanoparticles of Gold on TiO_2 Catalysts: A Cooperative Effect between Gold and the Support. *J. Am. Chem. Soc.* **2007**, *129*, 16230–16237.

38. Schwerdtfeger, P.; Boyd, P. D. W.; Brienne, S.; Burrell, A. K. Relativistic Effects in Gold Chemistry. 4. Gold(III) and Gold(V) Compounds. *Inorg. Chem.* **1992**, *31*, 3411–3422.

39. Govorov, A. O.; Zhang, H.; Gunko, Y. K. Theory of Photoinjection of Hot Plasmonic Carriers from Metal Nanostructures into Semiconductors and Surface Molecules. *J. Phys. Chem. C* **2013**, *117*, 16616–16631.

40. Janssens, T. V. W.; Clausen, B. S.; Hvolbaek, B.; Falsig, H.; Christensen, C. H.; Bligaard, T.; Norskov, J. K. Insights into the Reactivity of Supported Au Nanoparticles: Combining Theory and Experiments. *Top. Catal.* **2007**, *44*, 15–26.

41. Lyalin, A.; Taketsugu, T. A Computational Investigation of H_2 Adsorption and Dissociation on Au Nanoparticles Supported on TiO_2 Surface. *Faraday Discuss.* **2011**, *152*, 185–201.

42. Haiss, W.; Thanh, N. T.; Aveyard, J.; Fernig, D. G. Determination of Size and Concentration of Gold Nanoparticles from UV-Vis Spectra. *Anal. Chem.* **2007**, *79*, 4215–4221.

43. Sanz, J. M.; Ortiz, D.; Alcaraz de la Osa, R.; Saiz, J. M.; González, F.; Brown, A. S.; Losurdo, M.; Everitt, H.; Moreno, F. UV Plasmonic Behavior of Various Metal Nanoparticles

ARTICLE

in the Near-and Far-Field Regimes: Geometry and Substrate Effects. *J. Phys. Chem. C* **2013**, *117*, 19606–19615.

44. Albella, P.; Garcia-Cueto, B.; González, F.; Moreno, F.; Wu, P. C.; Kim, T.-H.; Brown, A.; Yang, Y.; Everitt, H. O.; Videen, G. Shape Matters: Plasmonic Nanoparticle Shape Enhances Interaction with Dielectric Substrate. *Nano Lett.* **2011**, *11*, 3531–3537.

45. Jain, P. K.; Lee, K. S.; El-Sayed, I. H.; El-Sayed, M. A. Calculated Absorption and Scattering Properties of Gold Nanoparticles of Different Size, Shape, and Composition: Applications in Biological Imaging and Biomedicine. *J. Phys. Chem. B* **2006**, *110*, 7238–7248.

46. Grammatikopoulos, S.; Pappas, S. D.; Dracopoulos, V.; Poulopoulos, P.; Fumagalli, P.; Velgakis, M. J.; Politis, C. Self-Assembled Au Nanoparticles on Heated Corning Glass by Dc Magnetron Sputtering: Size-Dependent Surface Plasmon Resonance Tuning. *J. Nanopart. Res.* **2013**, *15*, 1–8.

47. Stobiński, L.; Nowakowski, R.; Duś, R. Atomic Hydrogen Adsorption on Thin Discontinuous and Continuous Gold Films—Similarities and Differences. *Vacuum* **1997**, *48*, 203–207.

48. Aruda, K. O.; Tagliazucchi, M.; Sweeney, C. M.; Hannah, D. C.; Schatz, G. C.; Weiss, E. A. Identification of Parameters through Which Surface Chemistry Determines the Lifetimes of Hot Electrons in Small Au Nanoparticles. *Proc. Natl. Acad. Sci. U.S.A* **2013**, *110*, 4212–4217.

49. Link, S.; El-Sayed, M. A. Spectral Properties and Relaxation Dynamics of Surface Plasmon Electronic Oscillations in Gold and Silver Nanodots and Nanorods. *J. Phys. Chem. B* **1999**, *103*, 8410–8426.

50. Libisch, F.; Cheng, J.; Carter, E. A. Electron-Transfer-Induced Dissociation of H_2 on Gold Nanoparticles: Excited-State Potential Energy Surfaces *via* Embedded Correlated Wavefunction Theory. *Masthead* **2013**, 227.

51. Schmickler, W.; Santos, E. *Interfacial Electrochemistry*; Oxford University Press: New York, 1996; Vol. 134, p 13.

52. Thompson, C. V. Solid-State Dewetting of Thin Films. *Annu. Rev. Mater. Res.* **2012**, *42*, 399–434.

53. Necas, D.; Klapetek, P. Gwyddion: An Open-Source Software for SPM Data Analysis. *Cent. Eur. J. Phys.* **2012**, *10*, 181–188.

54. Draine, B. T.; Flatau, P. J. Discrete-Dipole Approximation for Scattering Calculations. *JOSA A* **1994**, *11*, 1491–1499.

55. Palik, E. D. *Handbook of Optical Constants of Solids*; Academic Press: New York, 1998; Vol. 3.

56. Plimpton, S. Fast Parallel Algorithms for Short-Range Molecular Dynamics. *J. Comput. Phys.* **1995**, *117*, 1–19.